

LIBRARY USE ONLY

TM96-2063

NUWC-NPT Technical Memorandum 962063

Naval Undersea Warfare Center Division
Newport, Rhode Island



**ANALYTICAL MODEL FOR THE VELOCITY AND POSITION MEASUREMENT
OF A HIGH-SPEED PROJECTILE**

C. P. Cho
W. P. Krol
Weapons Technology and Undersea Systems Department

1 August 1996

UNCLASSIFIED
NAVAL UNDERSEA WARFARE CENTER
DIVISION NEWPORT
NEWPORT, RHODE ISLAND 02841-1708
RETURN TO: TECHNICAL LIBRARY

Approved for public release; distribution is unlimited.

LIBRARY USE ONLY

ABSTRACT

This technical memorandum presents the results of analytical, numerical, and experimental studies predicting the velocity and position of a high-speed projectile. Velocity and position predictions were made using computer modeling and simulation to find a reliable and cost-effective velocity sensor. The two most popular magnetic field sensing devices, the copper wire sense coil and the Hall effect sensor, were examined. An axisymmetric, 2-D finite element analysis model was developed (1) to calculate the field distribution due to a permanent magnet embedded in a projectile and (2) to verify the analytical model. Experiments were conducted and confirmed the accuracy of both the analytical and finite element models.

ADMINISTRATIVE INFORMATION

Research, development, and testing were performed under the Naval Undersea Warfare Center (NUWC) Division, Newport Supercavitating High-Speed Bodies (SHSB) program; Program Manager, C. Curtis; Chief Engineer, I. Kirschner. Initial feasibility testing, assessment, and range development were supported by the NUWC Division Newport Bid and Proposal program. Research was sponsored by the Office of Naval Research (ONR) Undersea Weaponry Basic Research program, J. Fein, Program Manager. Development was sponsored by the ONR Undersea Weaponry Exploratory Development program, Program Manager, S. Beermann. Feasibility testing was sponsored by the Advanced Research Projects Agency, Program Manager, G. Jones.

The authors of this memorandum are located at the Naval Undersea Warfare Center, Newport, RI.

ACKNOWLEDGMENTS

The authors are grateful for the support and contributions of the members of the Thermal and Electric Propulsion Branch (Code 8231), especially D. Thivierge and H. Atwater for the testing setups and measurement.

TABLE OF CONTENTS

Section	Page
ABSTRACT	i
ADMINISTRATIVE INFORMATION	i
ACKNOWLEDGMENTS.....	i
LIST OF ILLUSTRATIONS	iv
LIST OF TABLES.....	iv
1 INTRODUCTION.....	1
2 COMPARISON OF SENSING DEVICES	1
3 ANALYTICAL MODELING	4
3.1 Permanent Magnet Modeling	6
3.2 Calculation of Magnetic Flux Density	9
3.3 Calculation of Induced Voltage (Back Electromotive Force)	10
4 FEA MODELING	14
4.1 Permanent Magnet Material Selection Using an FEA Model.....	16
4.2 Projectile Steel Material Selection Using an FEA Model.....	17
5 EXPERIMENTAL MEASUREMENTS	19
5.1 Sense Coil Measurements.....	19
5.2 Repeatability and Accuracy of Measurements.....	22
5.3 Hall Effect Sensor Measurements.....	22
6 CONCLUSION	23
REFERENCES.....	23

LIST OF ILLUSTRATIONS

Figure		Page
1	Sense Coil with a Moving PM.....	2
2	Electron Movement in a Hall Effect Device.....	2
3	Geometry Used in Developing the Magnetic Flux Equations	5
4	Permanent Magnet Model.....	7
5	Analytical Model of a Falling PM (Voltage Equation)	11
6	Generated Voltage as a Function of Time.....	12
7	Experimentally Measured Voltage as a Function of Time	12
8	Superimposed Experimentally Measured and Calculated Voltages.....	13
9	Generated Voltage as a Function of PM Position	13
10	2-D Axisymmetric FEA Model.....	14
11	Expanded View of the 2-D Axisymmetric FEA Model	14
12	Flux Distribution Plot.....	15
13	Magnetic Flux Density in the Axial Direction	15
14	Magnetic Flux Density in the Radial Direction.....	16
15	Magnetic Flux Density as a Function of Magnet Position (40 MGOe, 979 kA/m)	16
16	Magnetic Flux Density as a Function of Magnet Position (22 MGOe, 764 kA/m)	17
17	Flux Distribution Plot ($\mu_r=1.0$)	18
18	Flux Distribution Plot ($\mu_r=10.0$)	18
19	Permanent Magnet Drop-Test Setup Block Diagram.....	19
20	Permanent Magnet Drop-Test Setup Picture	20
21	Drop-Test Measurements with Three Permanent Magnets.....	20
22	Drop-Test Measurements with Seven Permanent Magnets	21
23	Shout-Test Measurements Test Setup.....	21
24	Voltage Varies Linearly with Flux Density	22

LIST OF TABLES

1	Advantages and Disadvantages of the Sense Coil	3
2	Advantages and Disadvantages of the Hall Effect Sensor	4
3	Parameters To Determine Generated Voltage.....	11

1. INTRODUCTION

The main focus of this particular research project was (1) to predict the velocity and position of a high-speed projectile that contains an embedded rare-earth permanent magnet (PM) using computer modeling and simulation and (2) to find a feasible, reliable, compact, and cost-effective electromagnetic motion-detection sensor.

This technical memorandum (TM) concentrates on the first aspect of the research: developing an analytical model that can predict velocity and position of a high-speed projectile. The application of and results obtained from two popular magnetic field sensing devices, the copper wire sense and the Hall effect sensor, are examined. Because these sensors must accommodate uncertainty in the actual trajectory of the projectile, the sensing elements must be located a significant distance from the ideal projectile path. This required distance reduces the magnetic field strength observed at the sensor, thus significantly complicating the measurement.

An analytical model was developed to predict the characteristics of the voltage waveform induced in a sense coil. That model also helped define the requirements of the data acquisition and peripheral instrumentation control electronics.

A finite element analysis (FEA) model was also developed to calculate the field distribution due to the PM embedded in the projectile and to verify the analytical model. Experiments were conducted using a low-speed (40 m/s) projectile. These measurements confirmed the accuracy of the analytical and FEA models.

2. COMPARISON OF SENSING DEVICES

The magnetic field sensor appropriate for a particular application depends on the performance, noise immunity, reliability, thermal management, economics, and packaging of the device. Sense coils (figure 1) and Hall effect sensors (figure 2) are the two most common methods of sensing the magnetic field of a moving PM and measuring the velocity and position of that PM. In most motion control applications, the sensor is part of a closed loop control system. In such an application, the sensor is fixed and external to the system: it simply measures the magnetic field due to a moving PM from a fixed distance.

The voltage induced in a simple sense coil is a function of the magnetic flux present at right angles to the conducting coil and the frequency of the time-varying magnetic field. This relationship is expressed as

$$V = -N \frac{d\phi}{dt}, \tag{1}$$

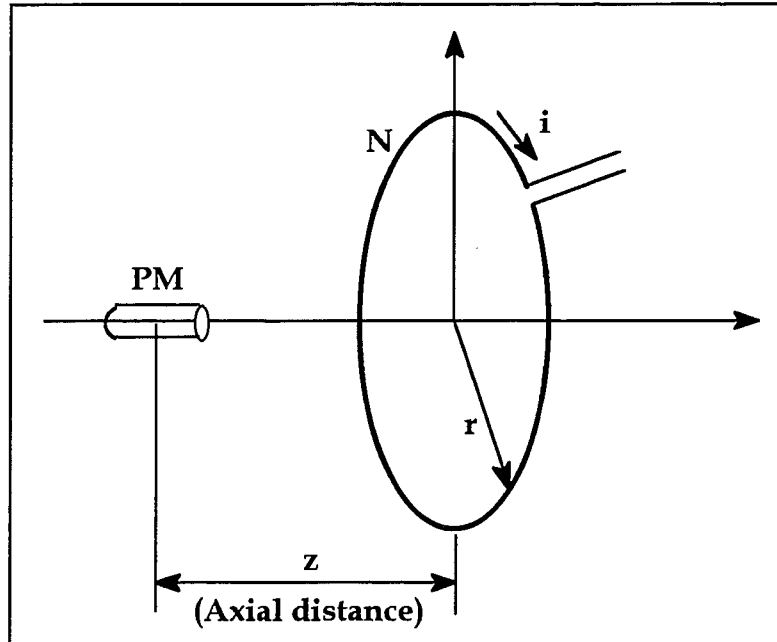


Figure 1. Sense Coil with a Moving PM

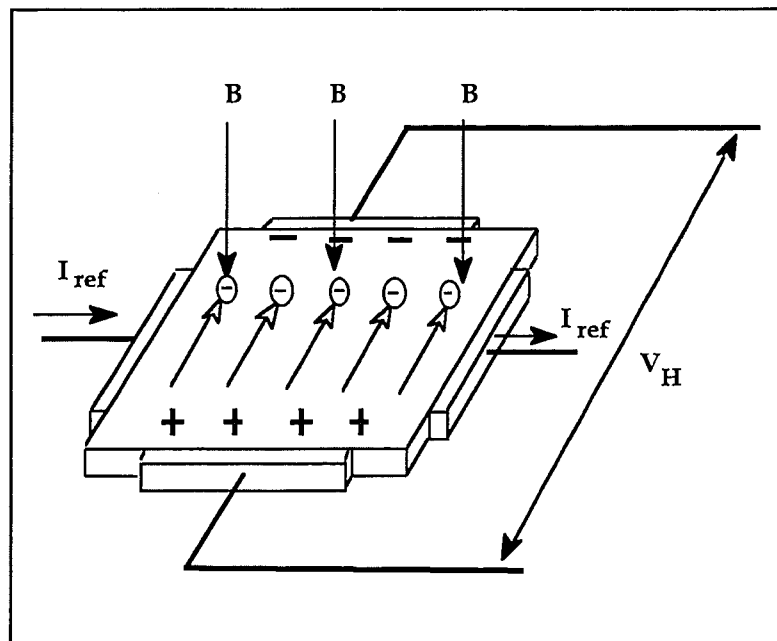


Figure 2. Electron Movement in a Hall Effect Device

where V is the generated voltage at the coil, N is the total number of turns in the coil, $\frac{d}{dt}$ is the total derivative operator, and ϕ is the magnetic flux exposed to the coil.

The Hall effect, discovered by E. F. Hall in 1879, is the basis for all Hall effect devices [1]. (A conceptual model for the basic principle of Hall effect sensor is shown in figure 2.) When a magnetic field B is applied perpendicularly to a current I_{ref} flowing in a semiconductor bar, an electric field is produced perpendicular to both B and I_{ref} (proportional to BI_{ref}) and an open-circuit voltage V_H is observed. The ratio V_H/V , where V is the applied voltage, is proportional to $\mu_H BI$, where μ_H is the Hall mobility. When this physical effect is combined with modern integrated circuit (IC) technology, many useful magnetic sensing devices are possible. The Hall element, when properly biased, produces an output voltage that is proportional to a magnetic field. To make a linear magnetic sensor, this small voltage is processed through a high-quality amplifier, which produces an analog output that is proportional to the applied flux density. The Hall voltage is defined by

$$V_H = \frac{R_H}{d} (\bar{I}_{ref} \times \bar{B}), \quad (2)$$

where V_H is the Hall voltage in volts, R_H is the Hall coefficient (device material dependent), d is the device thickness, \bar{I}_{ref} is the current across the device in amperes, and \bar{B} is the magnetic flux density incident on the device in gauss.

For the same current, electrons must travel faster in a poor conductor than they must in a good conductor, and the force (and thus the voltage) is proportional to speed. Modern Hall sensors use silicon for its high-resistance material characteristic and not for its switching and control capabilities. A typical Hall sensor of the linear variety may have a high resistance (about 1000 Ω) across the reference current leads and perhaps a little less resistance across the sense leads.

Table 1 summarizes advantages and disadvantages of the sense coil; table 2 summarizes those for the Hall effect sensor.

Table 1. Advantages and Disadvantages of the Sense Coil

ADVANTAGES	DISADVANTAGES
Extremely reliable	No built-in electrical isolation
No external power requirements	Comparatively large size and weight
Zero-output for zero-magnetic field temporal variation	Output amplification required
Output is a function of magnetic field frequency	Measures only time-varying magnetic fields
Easily understood in the context of Faraday's and Ohm's Laws	Comparatively expensive

Table 2. Advantages and Disadvantages of the Hall Effect Sensor

ADVANTAGES	DISADVANTAGES
Built-in electrical isolation	Magnetic field strength and power supply variations must be accounted for
Extremely small size and weight	Requires an external power supply
Very reliable	Offset for zero-magnetic field
Low cost	Less easily understood than sense coil
Measures both constant and time-varying magnetic fields	

3. ANALYTICAL MODELING

An analytical model, developed using the Biot-Savart law, Maxwell's field equations, and the Evershed model of PM bars, predicts the magnitude and frequency of the voltage waveform induced in a copper-wire sense coil. That model also helps define the requirements of the data acquisition and peripheral instrumentation control electronics for the experiment prior to actual high-speed projectile tests. The expense of those tests dictate that all issues regarding data acquisition and control be resolved before the start of testing.

Integration of the expression for the normal component of a magnetic dipole field was carried out over the area enclosed by a sense coil loop for horizontal orientation of the moment. The resulting formula for Φ , the magnetic flux linked to coil loop, is a function of (1) the dimensions of the coil loop, (2) the distance from the center of the loop to the dipole, and (3) the magnitude and orientation of the PM moment. Rectangular coordinates were used in which z was the axial distance of the moving permanent magnet m , and r was the radius of the coil loop (see figure 1).

A PM can be represented by a single magnetic dipole. Accordingly, the flux expressions were derived on that basis, taking into account the relative position of the coil loop and the position of the moving PM. A procedure was outlined for computing Φ when the PM dipole was oriented in an arbitrary manner or when it was desired to obtain Φ for a space-distribution of dipoles.

The effects of variations of strength, length, and diameter of the PM on Φ were studied, the results of which were used to determine the size of the coil loop for optimum response.

The magnetic induction at point P due to the presence of a small bar PM of pole strength q at the origin of the coordinate system (see figure 3) is given by

$$\vec{B} = \mu \vec{H} = (3\vec{M} \cdot \vec{r}\vec{r} - r^2 \vec{M})r^{-5}, \quad (3)$$

where $M = ql$ is the total magnetic moment of the PM, and l , its length, is much less than r (the magnitude of the radius vector r). If the quantities on the right side of equation (3) are measured in ampere/meter, B is in teslas.

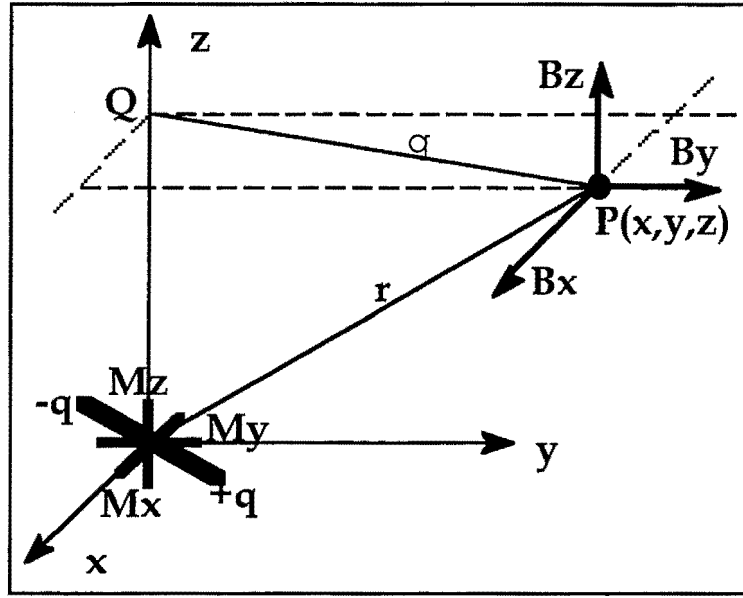


Figure 3. Geometry Used in Developing the Magnetic Flux Equations

The components of B with respect to any arbitrary Cartesian coordinate system with origin at point D are found by the usual methods of reduction to be

$$B_x = \mu H_x \frac{[M_x(3x^2 - r^2) + 3M_y xy + 3M_z xz]}{r^5}, \quad (4)$$

$$B_y = \mu H_y \frac{[3M_x yx + M_y(3y^2 - r^2) + 3M_z yz]}{r^5}, \quad (5)$$

and

$$B_z = \mu H_z \frac{[3M_x zx + 3M_y zy + M_z(3z^2 - r^2)]}{r^5}, \quad (6)$$

where, according to figure 3,

$$M_x = |M| \cos(\alpha),$$

$$M_y = |M| \cos(\beta),$$

$$M_z = |M| \cos(\gamma),$$

and

$$r^2 = x^2 + y^2 + z^2. \quad (7)$$

The quantity to be studied is the integral of B_z over a circular region in an xy -plane parallel to the coordinate XY -plane for special cases of the angles α , β , and γ . This integral predicts the magnetic field signatures from configurations of one or more permanent magnets.

3.1 PERMANENT MAGNET MODELING

A PM can be modeled as a magnetic dipole pair, with the strength of each pole ϕ equal to the flux through the central section of the magnet and the pole spacing l_p is almost equal to the magnet length. The magnet is assumed to be cylindrical with square-cut ends, axially magnetized, and made of a low permeability material (such as a ferrite or neodymium-boron-iron (Nd B Fe)).

Using the Evershed relationship, the demagnetizing factor, f_{DM} , can be calculated as

$$f_{DM} = \frac{2L}{D} \sqrt{1 + \frac{2}{D}}, \quad (8)$$

where D is the diameter of the PM and L is its length.

The magnetic moment of the test magnets were measured by inserting them into the working region of a Helmholtz Coil pair, with proper orientation. The coil was connected to an integrating fluxmeter. The meter was zeroed, and the magnet was then withdrawn a considerable distance and rotated 90° relative to the axis. The magnetic moment was then found from the product of the coil constant and fluxmeter reading, as described in reference 2.

In the mid-1800s, Ampere and others proved that steel bar magnets could be modeled as if they consisted of two poles of magnetic flux, a source (north or +) and sink (south or -), and that the flux travels in or out of the pole evenly in all directions (see figure 4).

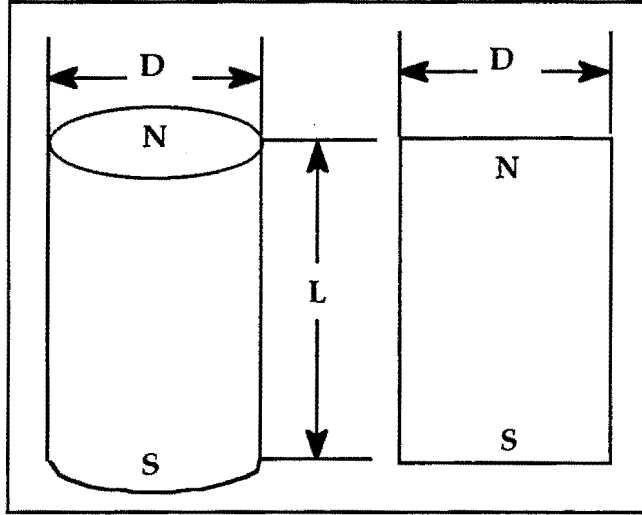


Figure 4. Permanent Magnet Model

$$\text{In general, } \phi = \frac{mmf}{R}, \quad (9)$$

where mmf is the magnetomotive force, R is the reluctance, and ϕ is the flux. If

$$\phi = \int B \cdot dA_x \quad (10)$$

and

$$mmf = \int H \cdot dl, \quad (11)$$

where B is the flux density, A_x is the cross-sectional area of the magnet, and H is the magnetic field intensity, it follows that

$$B \cdot A_x = \frac{H \cdot L_{eff}}{R} \quad (12)$$

and

$$\frac{B}{H} = \frac{L_{eff}}{A_x R}, \quad (13)$$

where L_{eff} is the effective distance between magnet poles.

$$\text{Set } L_{eff} = k_p \frac{L}{A_x R}, \quad (14)$$

where L is the magnet length and k_p is the ratio of pole spacing to total length

$$\frac{B}{H} = k_p \frac{L}{A_x R}. \quad (15)$$

Assuming the two poles behave independently, the reluctance in air is

$$R = \frac{1}{\mu_0} \int \frac{dl}{A_s}, \quad (16)$$

where A_s is a total spherical area. Because the flux is uniform in all directions,

$$A_s = 4\pi r^2 \quad (17)$$

and

$$R_{one\ pole} = \frac{1}{\mu_0} \int \frac{dr}{4\pi r^2} = \frac{1}{4\pi\mu_0} \int \frac{dr}{r^2} = \frac{1}{4\pi\mu_0} \left(\frac{1}{a} \right) - \frac{1}{4\pi\mu_0} \left(\frac{1}{b} \right). \quad (18)$$

The upper limit of integration should be set at infinity. If the lower limit is set at zero, the reluctance becomes infinite. Instead, assume a lower limit of a sphere of area A_s and radius r_s . The reluctance of one pole is then

$$R_{one\ pole} = \frac{1}{4\pi\mu_0 r_s}. \quad (19)$$

The total reluctance of both poles is therefore

$$R_{total} = \frac{1}{2\pi\mu_0 r_s}. \quad (20)$$

The area of one of the spheres is

$$\Lambda_s = 4\pi r_s^2 \quad (21)$$

and

$$r_s = \left(\frac{\Lambda_s}{4\pi} \right)^{\frac{1}{2}}. \quad (22)$$

The reluctance, in terms of sphere area, Λ_s , is

$$R = \frac{1}{2\pi\mu_0} \left(\frac{\Lambda_s}{4\pi} \right)^{-\frac{1}{2}}. \quad (23)$$

Setting the area of two spheres equal to the actual magnet area Λ_s ,

$$R = \frac{1}{\mu_0 \left(\frac{1}{2} \pi \Lambda_s \right)^{\frac{1}{2}}}, \quad (24)$$

where $A_s = 2\Lambda_s$. Substituting this result into the B/H formula,

$$\frac{B}{H} = k_p \frac{L\mu_0 \left(\frac{1}{2} \pi A_s \right)^{\frac{1}{2}}}{A_x}. \quad (25)$$

For a round bar magnet with square-cut ends,

$$\begin{aligned} A_s &= (\text{side area}) + 2 \cdot (\text{end area}), \\ A_s &= \pi DL + 2 \cdot \left(\frac{\pi}{4} D^2 \right), \end{aligned} \quad (26)$$

and

$$A_x = \frac{\pi}{4} D^2. \quad (27)$$

Substituting these results into equation (25),

$$\frac{-B}{\mu_0 H} = k_p \frac{4L}{\pi D^2} \left[\frac{1}{2} \pi \left(\pi DL + \frac{\pi D^2}{2} \right) \right]^{\frac{1}{2}} \quad (28)$$

and

$$\frac{-B}{\mu_0 H} = k_p \left(\frac{2L}{D} \right) \left(1 + \frac{2L}{D} \right)^{\frac{1}{2}}. \quad (29)$$

3.2 CALCULATION OF MAGNETIC FLUX DENSITY

The average flux density B can be found from the B/H curve of the permanent magnet material. If the recoil permeability of the magnet material is known, and if the B/H line remains in the linear region,

$$B_{Average} = B_r \left(\frac{1}{1 + \frac{\mu_r}{f_{DM}}} \right). \quad (30)$$

For ferrite and Nd-B-Fe, μ_r is about 1.04 to 1.08, and an average value is $\mu_r = 1.06$. The flux (equal to the pole strength) is

$$\phi = B_{Average} \cdot A_M, \quad (31)$$

$$A_M = \pi D^2. \quad (32)$$

The flux can be measured with a search coil closely fitting the magnet and an integrating fluxmeter. The magnetic moment m of the magnet is

$$m = \phi \cdot l_p, \quad (33)$$

where l_p is the spacing between equivalent poles.

3.3 CALCULATION OF INDUCED VOLTAGE (BACK ELECTROMOTIVE FORCE)

The voltage induced in a pickup coil is

$$E = N \frac{d\phi_c}{dt}, \quad (34)$$

where N is the number of coil turns and ϕ_c is the flux passing through the coil.

The flux linking a coil at distance z from a coil of radius r , from a magnetic dipole of strength m is calculated by assuming that at the positive (N) pole, the pole is a flux source, with flux ϕ radiating evenly in all directions. At the opposite (S) pole, a flux sink exists, and flux flows inward from all directions evenly (the total amount of which is ϕ).

As shown in reference 2,

$$\phi_c = m \left(\frac{1}{(r^2 + z^2)^{\frac{1}{2}}} - \frac{z^2}{(r^2 + z^2)^{\frac{3}{2}}} \right). \quad (35)$$

The voltage induced in the coil is expressed as

$$E = N \frac{d\phi_c}{dt} = N \frac{d\phi_c}{dz} \left(\frac{dz}{dt} \right), \quad (36)$$

where $\frac{dz}{dt}$ is the velocity of the magnet. It follows that

$$\frac{d\phi_c}{dz} = 3m \left(\frac{z^3}{(r^2 + z^2)^{\frac{5}{2}}} - \frac{z}{(r^2 + z^2)^{\frac{3}{2}}} \right), \quad (37)$$

$$E(N, r, z, v, L, D, B_r, \mu_r) = N \frac{d\phi_c}{dt},$$

and

$$= 3Nm \left(\frac{z^3}{(r^2 + z^2)^{\frac{5}{2}}} - \frac{z}{(r^2 + z^2)^{\frac{3}{2}}} \right) \left(\frac{dz}{dt} \right), \quad (38)$$

where N is the number of turns in a pickup coil, and r is its radius; z is the axial position of the PM, L is its length, D is its diameter, m is its moment, and μ_r is its permeability; and B_r is the remanent flux density.

Figure 5 shows an analytical model that calculates the EMF of a PM falling under the influence of gravity using the previously derived equations and data. A plot of generated voltage for the parameters given (table 3) is shown in figure 6 and corresponds well with the experimental data shown in figure 7. Figure 8 superimposes the experimentally measured and calculated voltages in single plot. Figure 9 re-plots the analytical data with respect to position.

$$E(z) := \left[\frac{z^3}{(r^2 + z^2)^{\frac{5}{2}}} - \frac{z}{(r^2 + z^2)^{\frac{3}{2}}} \right] \cdot 3 \cdot N \cdot M \cdot \sqrt{2 \cdot g \cdot (z - hl)} \quad t(z) := \sqrt{2 \cdot \frac{z - hl}{g}}$$

Figure 5. Analytical Model of a Falling PM (Voltage Equation)

Table 3. Parameters To Determine Generated Voltage

$N := 150$	Number of coil turns	$\pi := 3.14159265$	
$r := .23495$	Radius of coil	$h1 := -1.0$	Position 1
$g := 9.807$	Gravitation	$h2 := 1.0$	Position 2
		$z := h1, h1 + 0.01 .. h2$	
$d := \left(\frac{1}{4} \right) \cdot \frac{2.54}{100}$	Diameter of permanent magnet	$B_{avg} := -1.1564$	Permanent magnet flux density
		$d = 0.006$	
$l := (0.377) \cdot \frac{2.54}{100}$	Length of permanent magnet	$l = 0.01$	
$A := \frac{\pi}{4} \cdot d^2$	Permanent magnet cross-sectional area	$A = 3.167 \cdot 10^{-5}$	
$V := A \cdot l$	Permanent magnet volume	$V = 3.033 \cdot 10^{-7}$	
$M := B_{avg} V$	Magnet moment	$M = -3.507 \cdot 10^{-7}$	

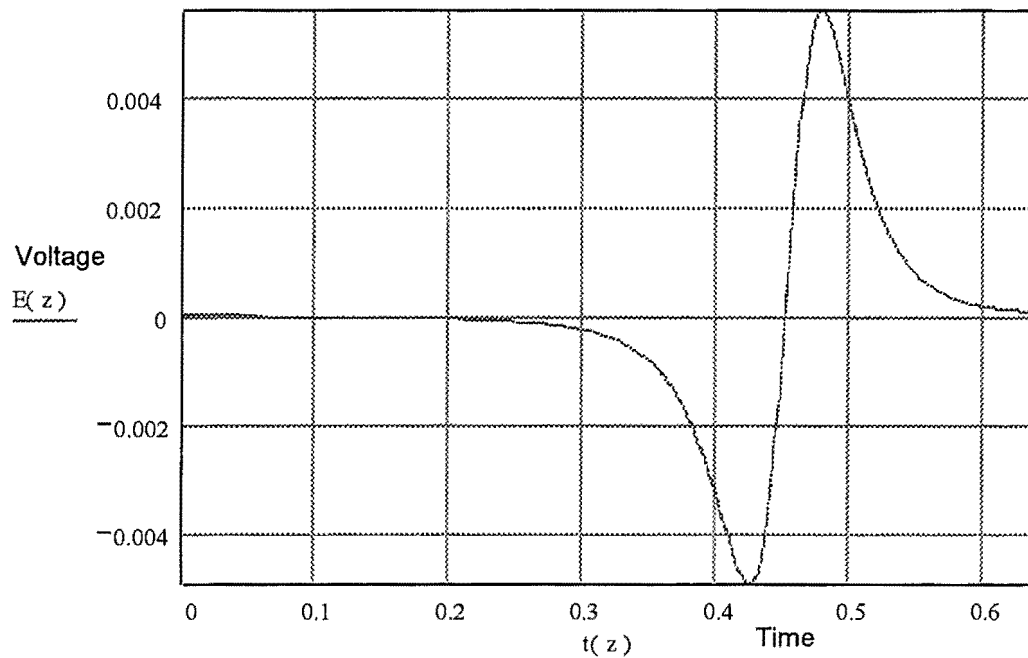


Figure 6. Generated Voltage as a Function of Time

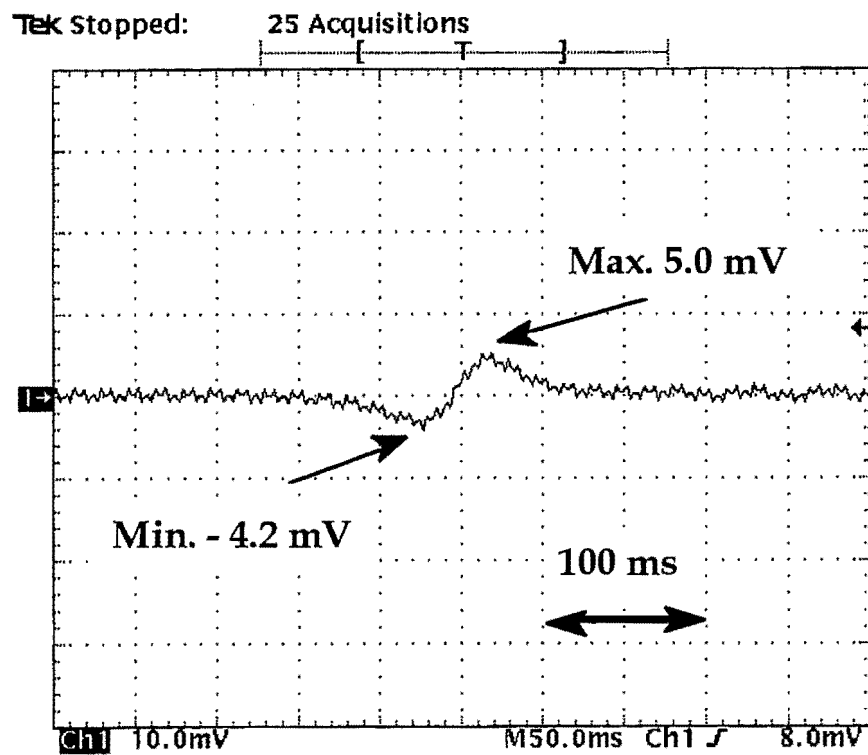


Figure 7. Experimentally Measured Voltage as a Function of Time

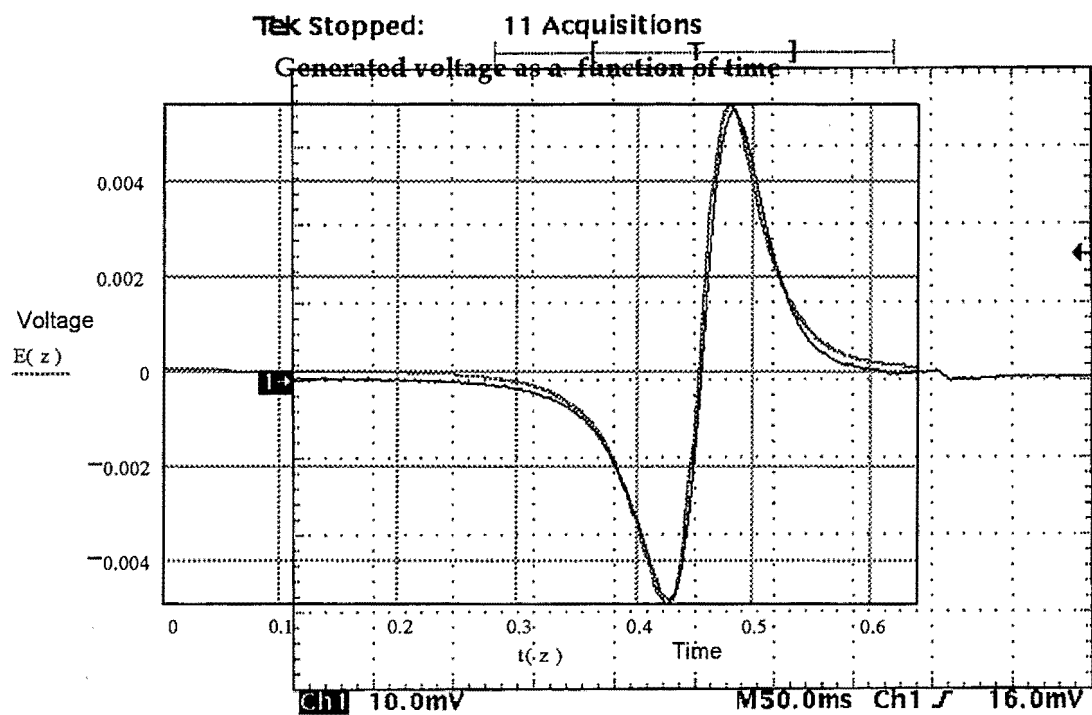


Figure 8. Superimposed Experimentally Measured and Calculated Voltages

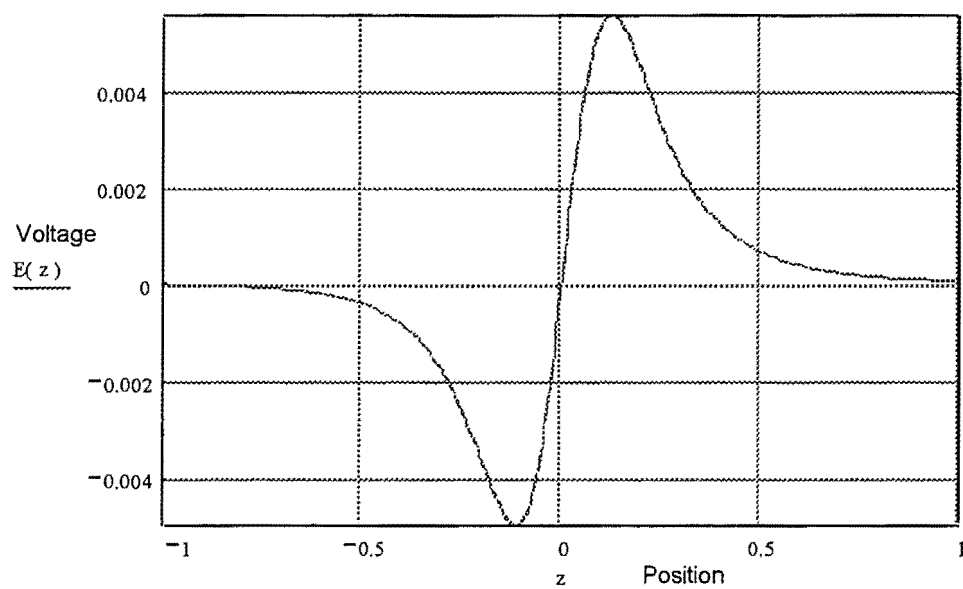


Figure 9. Generated Voltage as a Function of PM Position

4. FEA MODELING

A 2-D, axisymmetric FEA model was created and analyzed to calculate the magnetic flux distribution and to verify the analytical model and experimental measurements (references 3 and 4).

Figures 10 and 11 show the axisymmetric 2-D FEA model. The PM permeability and coercive force were obtained from the magnet distributor. The volume surrounding the PM measures 40 inches in the axial direction and 30 inches in the radial direction.

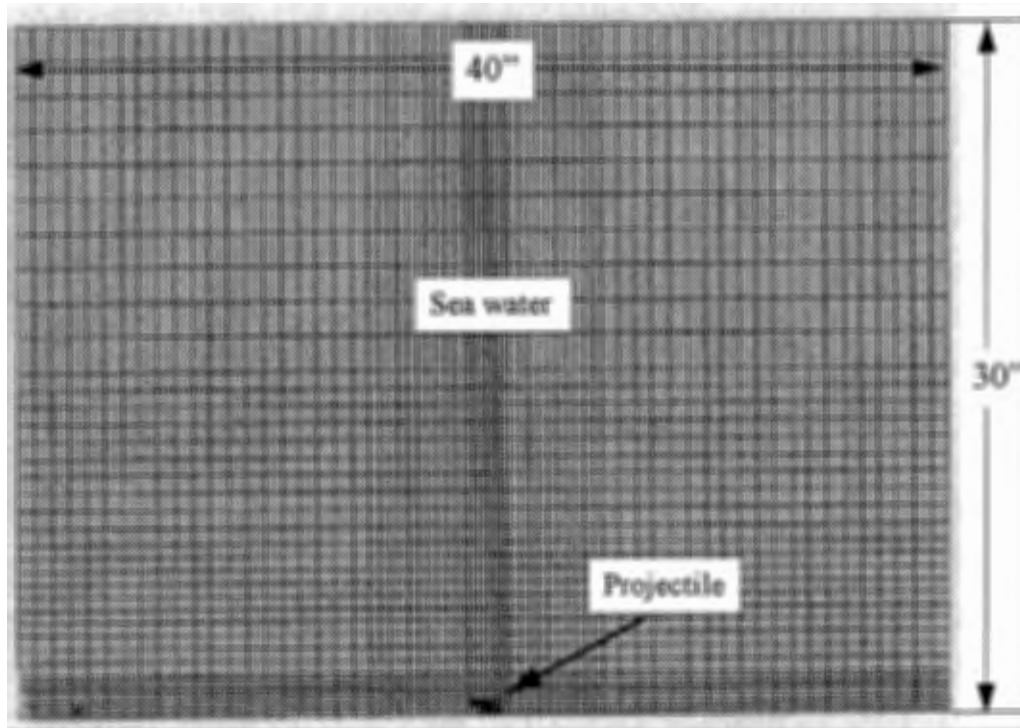


Figure 10. 2-D Axisymmetric FEA Model

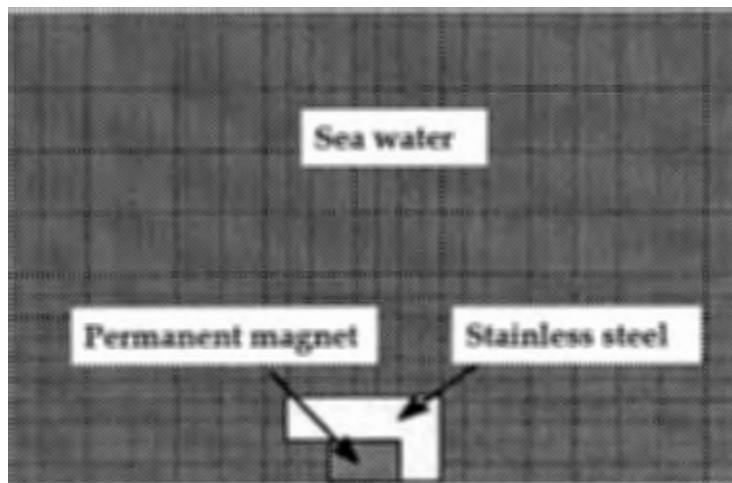


Figure 11. Expanded View of the 2-D Axisymmetric FEA Model

Figure 12 shows the magnetic flux lines in the surrounding volume that is shown in figure 11. Figures 13 and 14 illustrate the magnetic flux density in the axial and radial directions as a function of the radial distance from the PM. These FEA magnetic flux density calculations are compared with the analytical model and show close correlations.

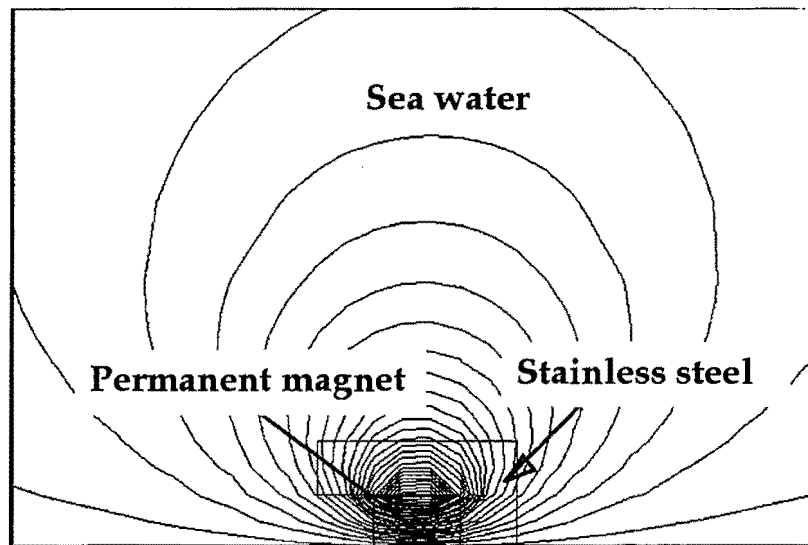


Figure 12. Flux Distribution Plot

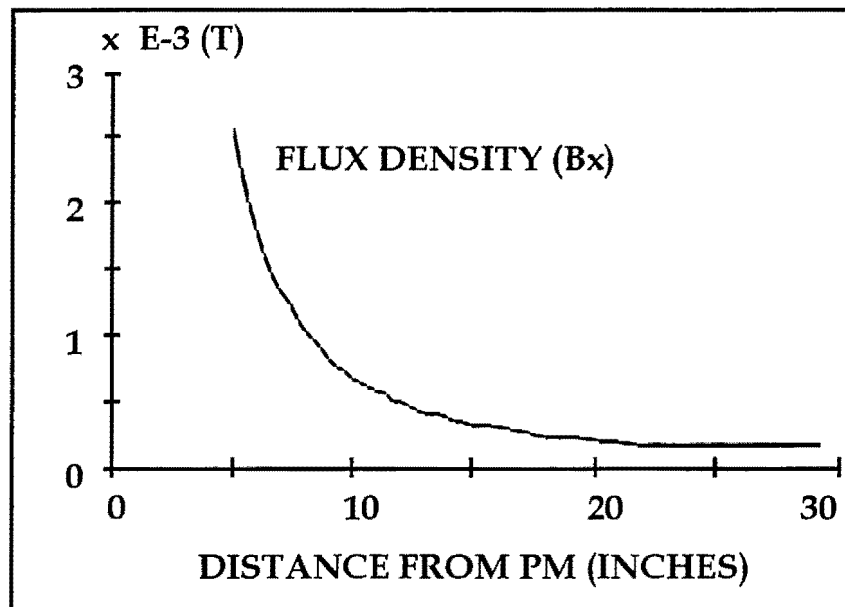


Figure 13. Magnetic Flux Density in the Axial Direction

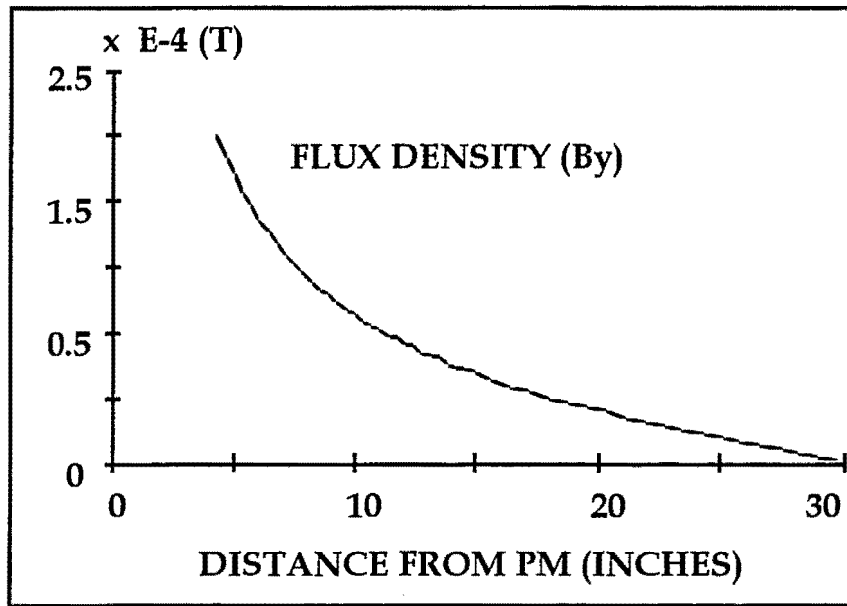


Figure 14. Magnetic Flux Density in the Radial Direction

4.1 PERMANENT MAGNET MATERIAL SELECTION USING AN FEA MODEL

An FEA model was built and analyzed to find the effect of PM material in the projectile. Figures 15 and 16 show the different results from two different PM strengths. The results in figure 15 from the 40 mega-gauss oersted (MGOe) with 979 kA/m Nd B Fe PM and the magnetic flux density are plotted as a function of the PM position. Figure 16 shows the results from the 22 MGOe, 764 kA/m PM material, revealing that the stronger PM produces a 15-percent higher magnetic field in the air around it. From those plots the maximum magnetic flux density was calculated.

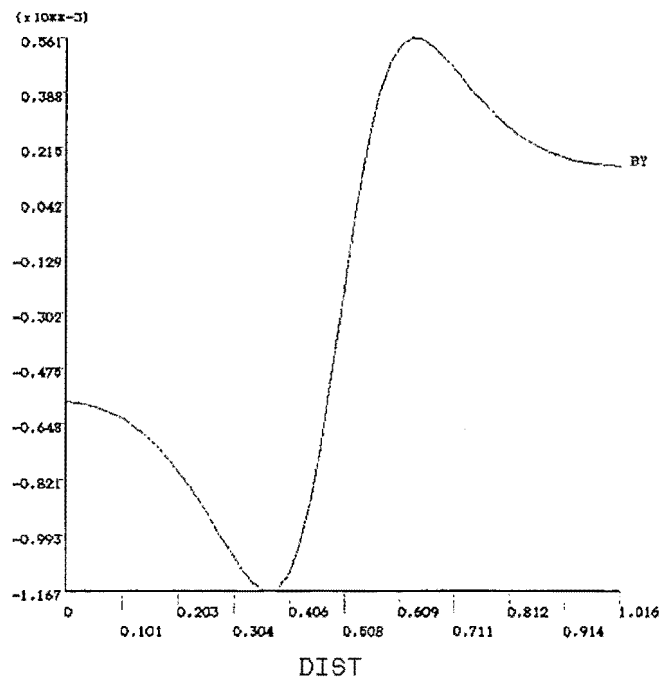


Figure 15. Magnetic Flux Density as a Function of Magnet Position (40 MGOe, 979 kA/m)

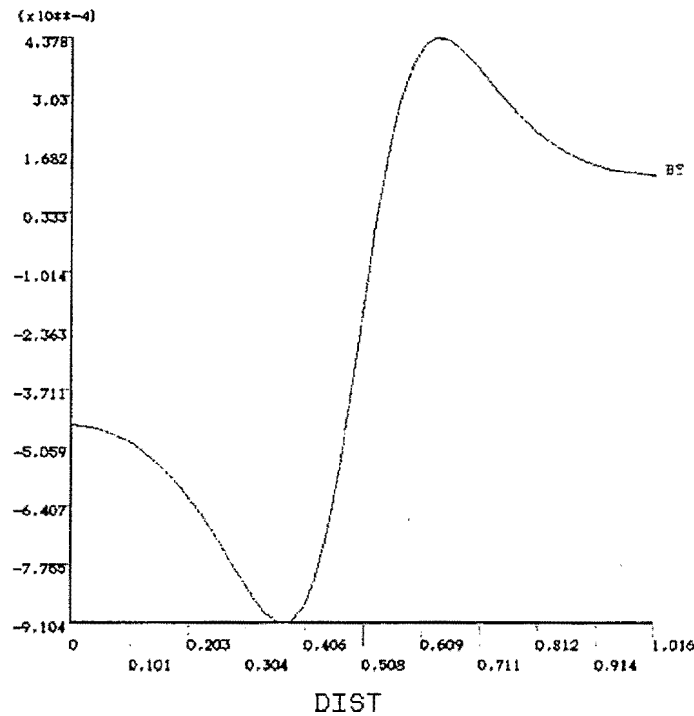


Figure 16. Magnetic Flux Density as a Function of Magnet Position (22 MGOe, 764 kA/m)

4.2 PROJECTILE STEEL MATERIAL SELECTION USING AN FEA MODEL

The FEA model was also used to find the appropriate material for the projectile. Permeability of the casing surrounding the PM was varied in appropriate intervals from 1.0 to 150. Higher permeability means that the magnetic flux encounters less reluctance; therefore, more flux flows in the material. In electric motor design, higher permeability materials are always preferable for flux concentration. In this project, however, a low permeability material is desired so that the flux is allowed to flow outside the projectile.

Figures 17 and 18 show the magnetic flux lines of the same PM strength but two different casings with permeabilities of 1.0 and 10.0 respectively. From these results, it was determined that permeability should be less than 5 to assure the broadest possible measurement range. Levels as high as 10 are still practical depending on the surrounding magnetic noise level.

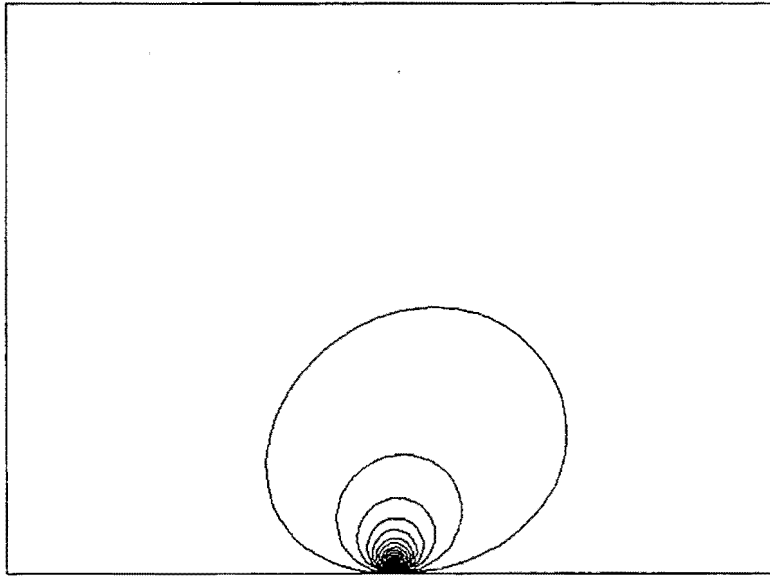


Figure 17. Flux Distribution Plot ($\mu_r = 1.0$)

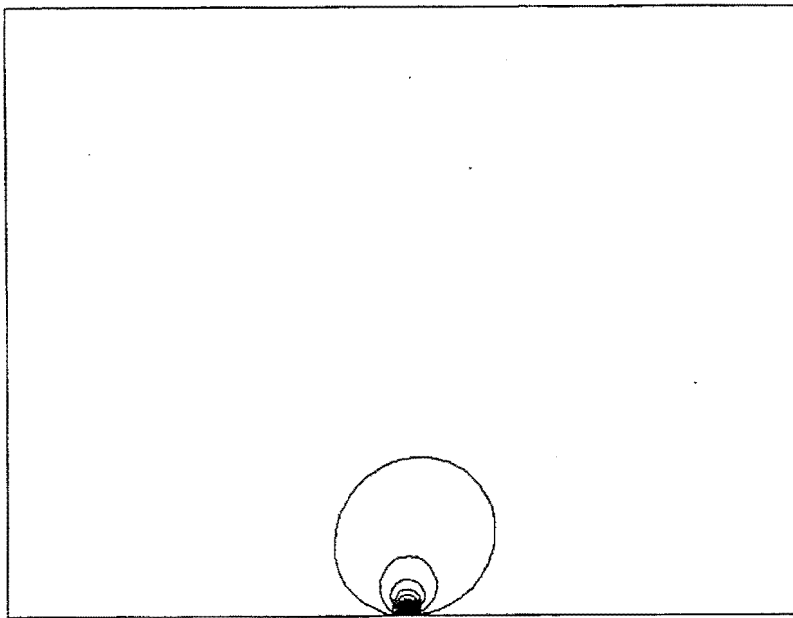


Figure 18. Flux Distribution Plot ($\mu_r = 10.0$)

5. EXPERIMENTAL MEASUREMENTS

5.1 SENSE COIL MEASUREMENTS

Experiments with the sense coil were conducted by first dropping a PM through the coil center and then shooting a PM projectile horizontally through the center of the coil using an air compressor. In both cases, the PM moved through a smooth glass tube. The analytical and FEA models developed proved to be an accurate means of predicting the induced voltage. From this calculated induced voltage, the position and speed of the projectile were determined.

Figure 19 shows a block diagram of the equipment used; figure 20 shows the test setup picture for the permanent magnet drop test. Several PM drop tests were performed and induced coil voltage waveforms recorded. Combinations of 1, 3, and 7 PMs attached in series were used for this experiment. Each PM was made of Nd B Fe and was cylindrical with dimensions of a 0.249-inch diameter and a 0.377-inch in length. Magnet poles were located at the top and bottom of the cylinders.

The results of a drop test using one PM is shown in figure 7. Measurements from tests with three and seven PM combinations are shown in figures 21 and 22. Figure 23 shows the shoot-test setup picture. The simulated and measured voltages were compared and showed about a 3-percent error between them.

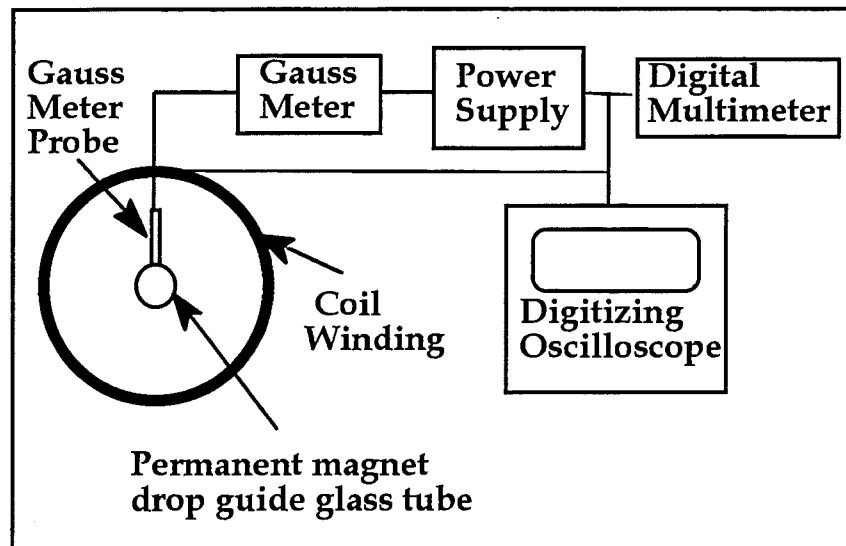


Figure 19. Permanent Magnet Drop-Test Setup Block Diagram



Figure 20. Permanent Magnet Drop-Test Setup Picture

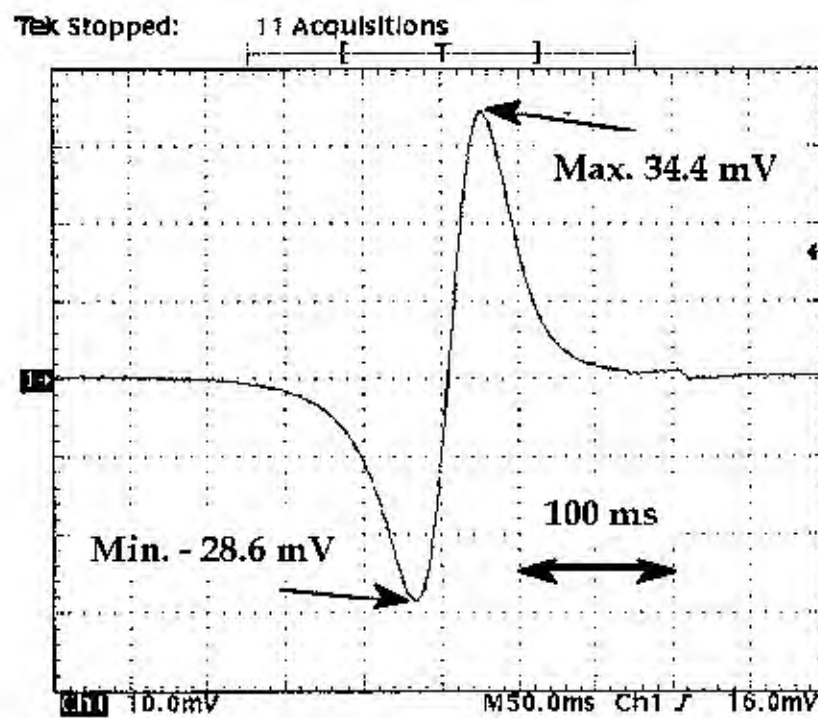


Figure 21. Drop-Test Measurements with Three Permanent Magnets

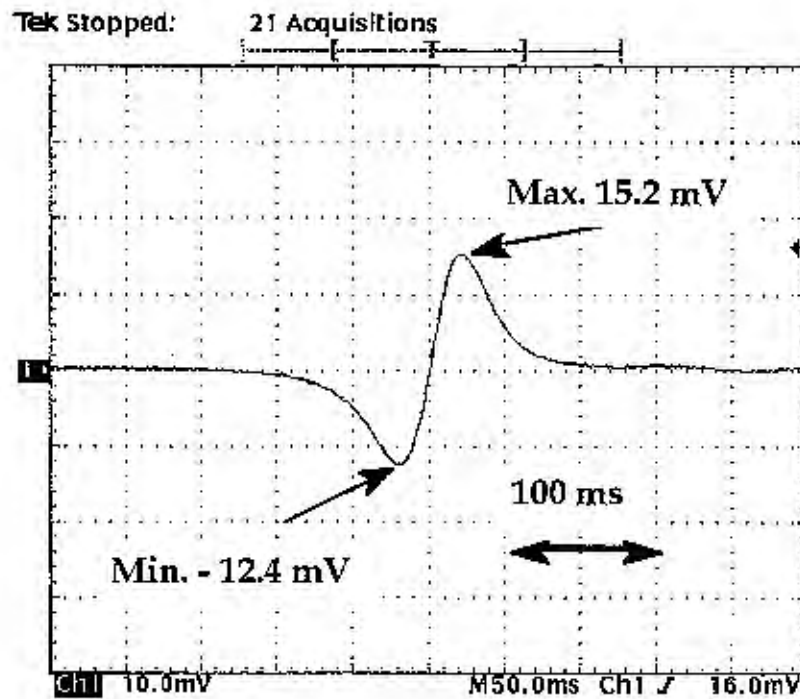


Figure 22. Drop-Test Measurements with Seven Permanent Magnets



Figure 23. Shout-Test Measurements Test Setup

5.2 REPEATABILITY AND ACCURACY OF MEASUREMENTS

Experimental test data it must be accurate and repeatable to be useful. A test was performed whereby the same set of data was recorded twice and the difference between the two was computed. The calculated differences were close to zero. The test was executed at several different speeds, and each time the results were nearly the same.

5.3 HALL EFFECT SENSOR MEASUREMENTS

Static flux density measurements were performed using a commercially available Hall effect sensor. Those measurements confirmed the manufacturer's claim that voltage varied linearly with flux density (figure 24). Because the sense coil experiments verified the results of the analytical and numerical models, no further experiments with moving PMs were performed.

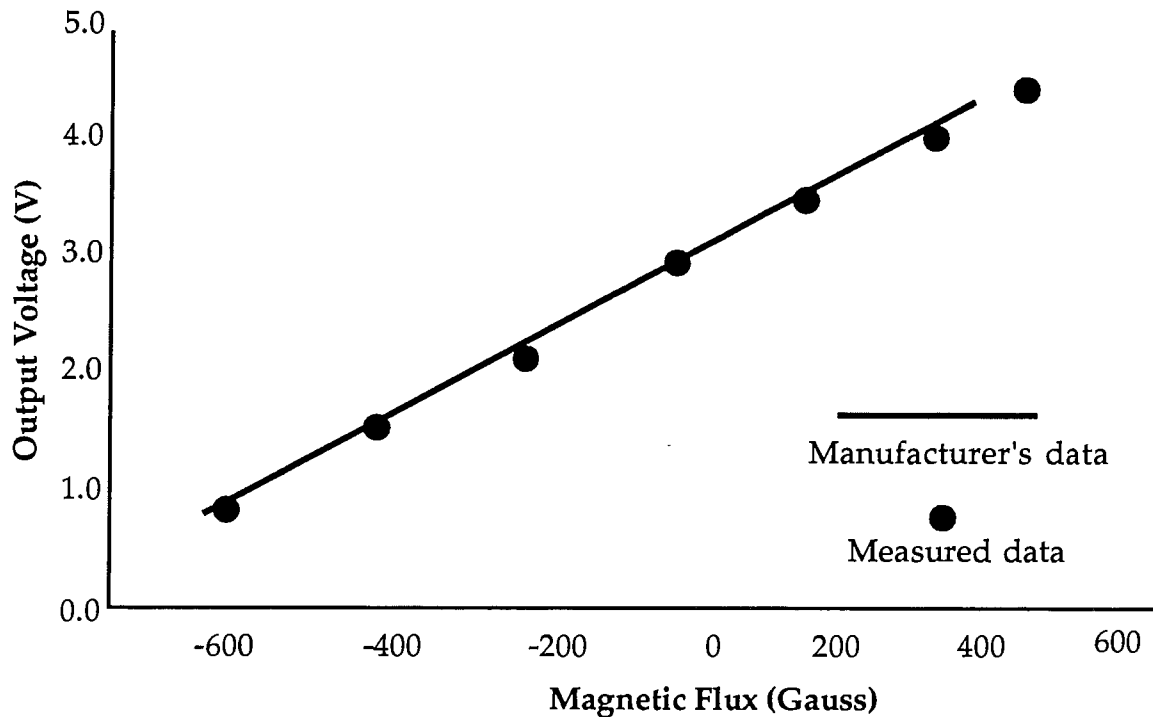


Figure 24. Voltage Varies Linearly with Flux Density

6. CONCLUSION

Analytical, numerical, and experimental techniques were combined to solve the problem of accurately determining the position and velocity of a high-speed projectile. First, an analytical model was created to predict the behavior of falling (low-speed) permanent magnets. This model and a more sophisticated FEA model were used to select appropriate materials and sensing equipment for running experiments. These experiments verified the analytical and numerical models, proving that the analytical and numerical models were also useful for sensing the behavior of high-speed projectiles.

REFERENCES

1. P. Emerard and J. Gilbert, "Introduction Theory and Fundamental of Hall Effect Sensor and Transducer," *IPCIM*, September 14, 1995.
2. J. Stupak, "A Method of Calibrating Helmholtz Coils for the Measurement of Permanent Magnets," *24th Annual Symposium, IMCSD*, June 1995.
3. D. Lowther and P. Silvester, *Computer-Aided Design in Magnetism*, Springer-Verlag, Berlin, New York, 1986.
4. M. Yaksh, "Electromagnetic Analysis of a Machine," ABB Impell Corporation, (in preparation).

DISTRIBUTION LIST

External

Internal

Codes: 01
0212
51122 (routing copy)
5131 (Conforti)
5141 (2)
10
102
104 (Keshura)
20
22
34
38
382
383
60
80
81
814
82
821
822
8222
8224
8225
823
8231 (Barnett, Cho (5), Egan, Raposa, Thivierge, Atwater)
8232
8233
8234
8291 (Benson, Cancilliere, Hillenbrand)
8292
83
832
8322 (Curtis (1), Kirschner (1))
833

Total: 48